Optical Pump-Probe Detection of Manganese Hyperfine Beats in (Cd,Mn)Te Crystals

S. Cronenberger,[1] M. Vladimirova,[1] S. V. Andreev,[1] M. B. Lifshits,[1,2] and D. Scalbert[1]

[1]*Laboratoire Charles Coulomb UMR 5221 CNRS/UM2, Université Montpellier 2, Place Eugene Bataillon, 34095 Montpellier Cedex 05, France*

[2]*Ioffe Physical-Technical Institute of the RAS, 26, Politechnicheskaya, 194021 Saint-Petersburg, Russia*

(Received 10 October 2012; published 14 February 2013)

Optical pump-probe experiments reveal spin beats of manganese ions in (Cd,Mn)Te, due to hyperfine and crystal fields. At ''magic'' orientations of the magnetic field, the effect of local crystal field is strongly suppressed. In this case, the spin precession of Mn^{2+} embedded in the lattice approaches the precession expected for the free ion. Following optical excitation, regular spin pulses show up, revealing the one-to-one correspondence between precession frequency and Mn^{2+} nuclear spin state. The period of the spin pulses accurately determines the hyperfine constant $|A| = 705$ neV. The manganese spin coherence time up to $T_2^{\mathrm{Mn}} \simeq 15$ ns is measured for a manganese concentration $x = 0.0011$.

DOI: 10.1103/PhysRevLett.110.077403 PACS numbers: 78.47.jm, 71.70.Jp, 72.25.Fe, 78.20.Ls

Manipulation of spin has become a very active field of research, exploiting quantum mechanical phenomena, such as superposition of states [1], entanglement among spins [2,3], quantum measurement at the single spin level [4], and spin squeezing [5,6].

Nuclear spin in semiconductors is very attractive to explore these phenomena, because it has very long coherence times [7,8], and can be controlled via the hyperfine interaction with electrons [9]. Manganese ions trapped on a semiconductor lattice have uniform properties and relatively long spin lifetimes, which make them promising for optical manipulation [10]. Both optical and electrical control, as well as optical readout, of single manganese spins has been done in II-VI [11] and III-V quantum dots [12]. Mn^{2+} ions embedded in a II-VI semiconductor are S-state ions possessing an electron spin $S = 5/2$ and a nuclear spin $I = 5/2$. At low manganese concentration, Mn^{2+} nuclear and electron spins are both very well protected against decoherence [13,14], and read-out of the nuclear spin via the hyperfine coupling between the nucleus and the $3d^5$ electrons should be possible.

In this Letter, we demonstrate the influence of hyperfine and crystal fields on the Larmor precession of the Mn^{2+} ion, by time-resolved Kerr rotation (TRKR) experiments. By choosing appropriate magnetic field orientation, we establish a one-to-one correspondence between the observed precession frequency and the nuclear spin state, enabling Mn^{2+} nuclear spin optical readout. Our results suggest that, ultimately, single Mn^{2+} spin can be detected by Kerr or Faraday rotation.

We begin with the model, which describes the time evolution of the average Mn^{2+} spin in the hyperfine and crystal fields. It is based on the spin Hamiltonian assessed by electron paramagnetic resonance experiments [15]

$$H = \hbar\omega \cdot \mathbf{S} + A\mathbf{I} \cdot \mathbf{S} + \frac{a}{6}\Big[S_x^4 + S_y^4 + S_z^4 - \frac{1}{5}S(S+1)(3S^2+3S-1)\Big]. \quad (1)$$

Below, the magnetic field direction will be specified by the polar angles (θ, φ), with respect to the crystal fourfold axes (x, y, z). The right-hand-side terms are the Zeeman, the hyperfine, and the crystal field terms, respectively. $\omega = g_{\mathrm{Mn}}\mu_B\mathbf{B}/\hbar$, $\mathbf{B}$ is the magnetic field, g_{Mn} is the Mn^{2+} Landé factor, and μ_B is the Bohr magneton. Prior to optical excitation, a thermal distribution of the Mn^{2+} states, described by the density matrix ρ_e, is assumed. Previous work has shown that the Mn^{2+} spin can be coherently rotated by a short optical tipping pulse [16–19]. The tipping pulse results from the exchange coupling terms between the Mn^{2+} d-electrons and the carriers excited by the laser. We assume an infinitely short tipping pulse, propagating along the direction $\mathbf{k}_t \perp \mathbf{B}$. At $t = 0$ it rotates the Mn^{2+} spin $\mathbf{S}$ by a small angle ϵ, so that the density matrix right after the tipping pulse becomes $\rho_i = \rho_e + i\epsilon[\rho_e, (\mathbf{k}_t/k_t)\cdot\mathbf{S}]$. At $t > 0$ the Liouville equation, including Lindblad term with a single relaxation time T_2^{Mn}, yields the time-evolution of the density matrix $\rho(t) = e^{-iHt/\hbar}[(\rho_i - \rho_e)e^{-t/T_2^{\mathrm{Mn}}} + \rho_e]e^{iHt/\hbar}$. The measured Kerr rotation is proportional to the Mn^{2+} spin component $S_p = \mathrm{Tr}[(\mathbf{S}\cdot\mathbf{k}_p/k_p)\rho(t)]$, parallel to the probe beam direction $\mathbf{k}_p$.

Figures 1(a) and 1(b) shows the envelope of S_p given by the numerical solution of this model when $T_2^{\mathrm{Mn}} = \infty$, for different magnetic field orientations and temperatures. For ''magic'' orientations of the magnetic field, the envelope of S_p assumes the form of a periodic train of spin pulses with the period $2\pi\hbar/A$ [black curves in Figs. 1(a) and 1(b)]. For any other field direction, the spin precession pattern becomes irregular and temperature dependent, as demonstrated in Figs. 1(a) and 1(b). The temperature dependence of S_p envelope is also illustrated in Fig. 1(c). It shows that

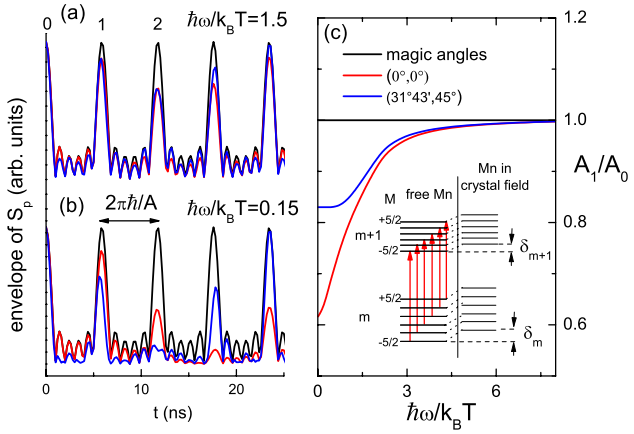

FIG. 1 (color online). (a, b) Calculated coherent evolution of the transverse Mn spin for different magnetic field orientations, in case of high ($\hbar\omega/k_BT = 1.5$) and low ($\hbar\omega/k_BT = 0.15$) polarizations, and for $T_2^{\mathrm{Mn}} = \infty$. (c) Amplitude of the first spin pulse normalized to the initial amplitude versus $\hbar\omega/k_BT$, for three different field orientations. The inset in (c) shows a scheme of the two lowest Zeeman levels, split into six hyperfine sublevels. The crystal field introduces a relative shift of Zeeman levels $\delta_{m+1} - \delta_m \sim -0.15$ GHz. The red arrows indicate the allowed spin-flip transitions.

the amplitude of the first spin pulse normalized to the amplitude at $t = 0$, varies with temperature except at magic angles. This effect must be considered for reliable estimation of the temperature dependence of T_2^{Mn}.

To get deeper insight, we calculate the Mn^{2+} spin levels to first order in $A/\hbar\omega$ and $a/\hbar\omega$

$$E_{mM} = (\hbar\omega + AM)m + \frac{a}{192}(5\sin^4\theta(7 + \cos 4\varphi) - 40\sin^2\theta + 8)(7m^4 + (5 - 6S(S+1))m^2). \quad (2)$$

Here, m and M label the electron and the nucleus spin projections along the magnetic field, respectively. Therefore, at any angle φ, there exists a magic angle $\theta_M(\varphi)$ satisfying $5\sin^4\theta(7 + \cos 4\varphi) - 40\sin^2\theta + 8 = 0$, such that the crystal field term vanishes [20,21]. In this case the Larmor precession spectrum consists in a frequency comb containing six evenly spaced lines at frequencies $\hbar\omega + AM$ [red arrows in Fig. 1(c)], which sets a one-to-one correspondence between precession frequency and nuclear spin state. In the time domain it corresponds to a periodic train of spin pulses with envelope $|\sin(\frac{2I+1}{2}\frac{At}{\hbar})/\sin(\frac{1}{2}\frac{At}{\hbar})|$, with the period $2\pi\hbar/A$, which depends neither on temperature, nor on crystal field. This envelope presents a sequence of strong peaks, and $2I - 1$ weak peaks in between.

For any other orientation, the crystal field introduces small shifts δ_m, and level mixing. At $T = 0$ only the lowest Zeeman level $m = -5/2$ is populated, one thus expects a rigid shift of the frequency comb by a small amount $\delta_{-3/2} - \delta_{-5/2} \sim -0.15$ GHz [inset in Fig. 1(c)], not affecting the spin pulses. At finite temperature, when higher Zeeman sub-levels are populated, the coherent spin evolution becomes irregular.

To check experimentally these ideas, we selected a bulk $Cd_{1-x}Mn_xTe$ sample with concentration low enough to resolve the fine and hyperfine structures of EPR spectra (not shown). The sample was cleaved along a (110) plane. The magnetic field is applied parallel to the (110) plane ($\varphi = \pi/4$), and the angle θ could be adjusted by rotating the sample around the $[1\bar{1}0]$ axis [22].

The effective Mn^{2+} concentration is estimated from the free-exciton spin splittings measured in Faraday configuration for the two circular polarizations [Fig. 2(b)]. As the spin splittings are small, only the strong exciton component is clearly resolved in each polarization. From the measured splitting $\Delta E = N_0(\alpha - \beta)x\langle S_z\rangle$ ($\langle S_z\rangle$ is proportional to the Brillouin function for spin $S = 5/2$), and the values of the sp-d exchange integrals $N_0\alpha = 220$ meV and $N_0\beta = -880$ meV, we deduce $x = 0.0008$. The photoluminescence spectra confirm that the sample is of p-type [Fig. 2(a)].

The spin precession is detected by time-resolved Kerr rotation (TRKR), with $\mathbf{k}_t$ and $\mathbf{k}_p$ nearly parallel to the $[1\bar{1}0]$ axis. The tipping pulse is resonant with the free-exciton transition [see Fig. 2(a)], well below the band gap, thus exciting only spin polarized free excitons. The probe pulse is slightly detuned below the free-exciton resonance, thereby maximizing the Kerr rotation signal. The pulse durations are about 0.5 ps, the repetition rate is 82 MHz, and the laser spot size is ~ 100 μm.

Figure 3 summarizes the main features of the observed TRKR signal at an angle $\theta = 30°$ close to the magic angle. At $t < 40$ ps (region I in Fig. 3) the TRKR signal $\theta_K(t)$ is

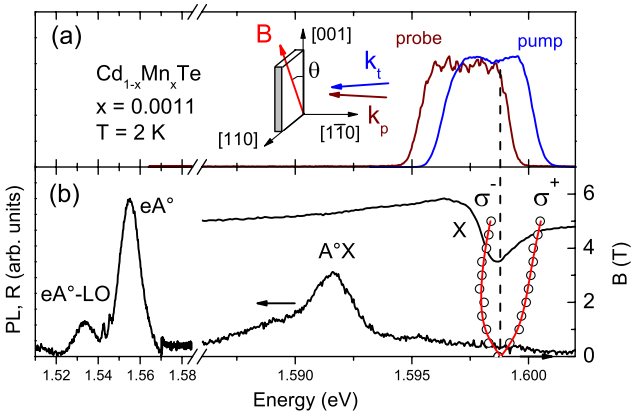

FIG. 2 (color online). (a) Pump-probe configuration and spectrally filtered pump (blue line) and probe pulses (wine line). (b) Left scale: Photoluminescence (PL) and reflectivity spectra (R). PL spectrum is dominated by acceptor bound excitons ($A°X$) and electron-acceptor recombination ($eA°$), which confirms that the sample is of p type [35]. The dispersivelike reflectivity feature (X) corresponds to the free-exciton transition. Right scale: measured exciton spin-splitting (circles) and fits (red curves) versus magnetic field.

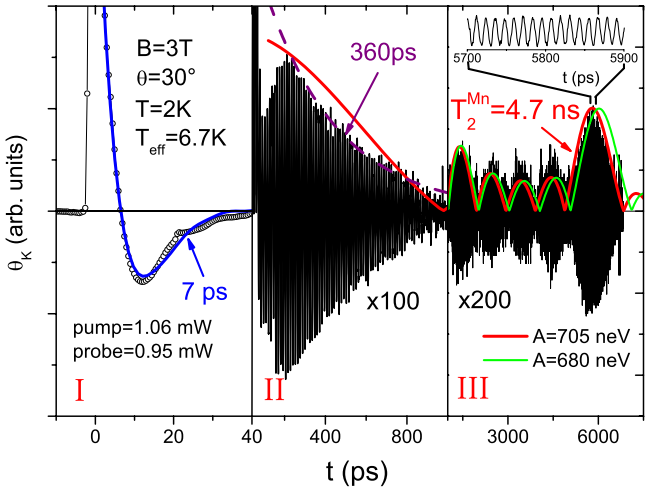

FIG. 3 (color online). Time-resolved Kerr rotation recorded at $\theta = 30°$. Three time intervals are distinguished: (I) signal dominated by free excitons spin precession, (II) signal dominated by Mn^{2+} spin precession, and (III) Mn^{2+} spin precession after exciton recombination (the inset shows an enlarged view of these oscillations). In (II) the dashed line is an exponential fit of the envelope of the precession. The red and green envelopes are calculated for two different values of the hyperfine coupling.

dominated by the contribution of free excitons and can be fitted to an exponentially decaying cosine, as $\theta_K(t) = A_e e^{-t/T_2^e} \cos(\omega_e t + \phi)$. $\omega_e(B)$ is fitted to a linear Zeeman term, plus an exchange term proportional to a $S = 5/2$ Brillouin function [see Fig. 4(a)]. From the fit we obtain $g_e = -1.62$ in agreement with the Landé factor of conduction band electrons [23], $x = 0.0011$ close to the concentration deduced from magneto-reflectivity experiments, and the effective Mn^{2+} spin temperature $T_{\text{eff}} = 3.8$ K. Although excitons are being involved, they behave as bare electrons, because of the fast hole spin flips [24]. Note that at $B \sim 6$ T the external and exchange fields compensate each other, so that the total field acting on the electron is zero. As in zero field, the electron spin coherence time T_2^e reaches a maximum [see Fig. 4(b)]. A maximum in T_2^e at zero field was also observed in DMS quantum wells [16,17], but is not explained by existing electron spin relaxation theory [25].

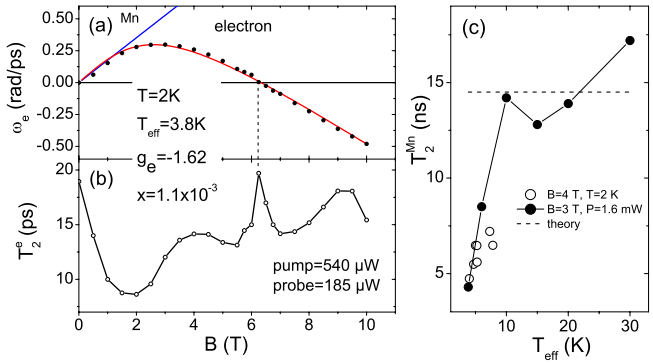

FIG. 4 (color online). (a) Electron spin precession frequency versus magnetic field. Red line is a fit to the data (circles). Blue line corresponds to the Mn^{2+} precession frequency. (b) Electron spin relaxation time. (c) Mn^{2+} spin relaxation time versus effective spin temperature T_{eff}. T_{eff} was varied either by changing the helium bath temperature (close circles), or by changing the optical excitation power (open circles). The dashed line shows the prediction based on dipolar broadening mechanism.

At $40 < t < 900$ ps (II) free excitons have lost their spin polarization, revealing the 2 orders of magnitude weaker Mn^{2+}-induced Kerr rotation ~ 1 μrad. Surprisingly, the amplitude of oscillations first increases up to 200 ps, and then decays exponentially up to 900 ps. This behavior is not consistent with the model of coherent precession (red curve), even if one considers an eventual nonthermal nuclear spins distribution. Note that the initial increase is clearly seen only at magic angle (see Fig. 5) and at $T = 2$ K. Although magnetic polaron formation is known to enhance locally the Mn^{2+} magnetization on subnanosecond time scales [26], it is not expected at the low Mn^{2+} concentration considered here. The detailed study of this puzzling effect is beyond the scope of this Letter.

At $t > 900$ ps (III) several Mn^{2+} spin beats show up, the strongest one being centered at $t = 5.86$ ns. It can be identified as pulse denoted 1 in Fig. 1(a). This fixes accurately the value of the hyperfine constant $|A| = 2\pi\hbar/t = 705$ neV in quite good agreement with Ref. [27]. The model accounts accurately for all the pattern of spin beats (red curve). It allows us to determine $T_2^{\text{Mn}} = 4.7 \pm 0.3$ ns, with the precision limited by the accuracy of 2° in sample orientation. Pulse 2 in Fig. 1(a) expected at $t \sim 12$ ns was hardly detected. This is because its amplitude is reduced both by spin relaxation, and by the eventual misorientation.

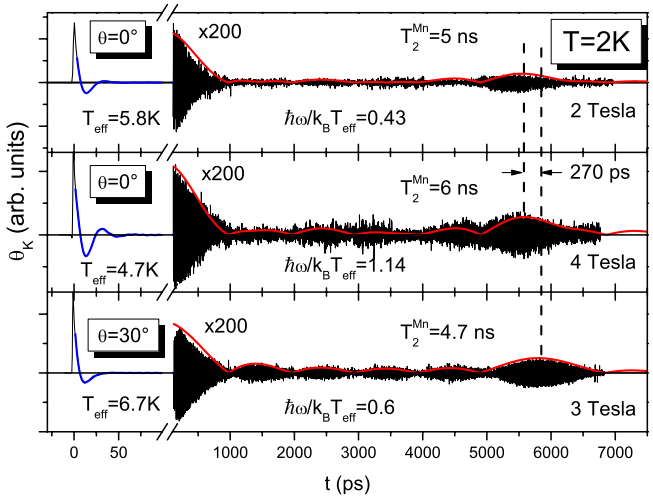

FIG. 5 (color online). Time-resolved Kerr rotation at different fields, and sample orientation. $\theta = 30°$ is close to the magic angle. The blue line is a fit of the initial time evolution dominated by free excitons, while the red line is a fit of the envelope of the Mn^{2+} precession (see text).

Finally, the inset shows a zoom on the Mn^{2+} spin precession corresponding to $g_{Mn} = 1.998 \pm 0.006$ in good agreement with previous determinations [27].

We now examine the effect of the crystal field on the Mn^{2+} spin dynamics by rotating the sample at $\theta = 0°$, where crystal field splittings are maximum. In Fig. 5 we compare the spin beats pattern measured at $\theta = 0°$ for two different values of magnetic field (upper curves), with the pattern measured at $\theta = 30°$ (lower curve). As predicted by the model, the spin beats pattern is less regular at $\theta = 0°$ than at magic angle, and becomes dependent on $\hbar\omega/k_B T_{\text{eff}}$. The crystal field also affects the delay at which the spin pulse 1 builds up. This results from interferences between the different components of the slightly irregular frequency comb. One can estimate that during the spin pulse lasting $\sim$1 ns, and for $\delta_{m+1} - \delta_m \sim \pm 0.15$ GHz the dephasing between the different components of the frequency comb reaches $\sim$2 rad. This explains why at $\theta = 0°$ the spin pulse 1 forms $\sim$270 ps earlier than at magic angle. The best agreement with the model is obtained for $a = 370$ neV, consistent with Ref. [27]. An important concern in optical spin manipulation is to identify the mechanism by which the Mn^{2+} spins are coherently rotated, and its efficiency. In previous work two mechanisms have been proposed. The coherent rotation in the field of the spin polarized holes [16,18,19], and rotation induced by spin-flip Raman scattering [3]. These mechanisms can be distinguished by the different phase imparted to the Mn^{2+} precession after spin relaxation of the carriers. The phase of the Mn^{2+} spin precession (not shown) corresponds to an initial rotation of the magnetization perpendicular to the pump beam direction, only consistent with the coherent rotation in the field of carriers. In this case, an estimate of the Kerr rotation angle is $\theta_K \simeq \sigma_K N_0 x \ell \omega_h \tau_h$, where σ_K is the Kerr rotation cross section, $\ell \sim 1$ μm is the penetration depth of light in the sample, ω_h is the Larmor frequency of Mn^{2+} in the field of holes $B_h \sim 1.6$ mT, and $\tau_h \sim 0.1$ ps is the hole spin relaxation time [28]. From the measured Mn^{2+}-induced Kerr rotation $\theta_K \sim 1$ μrad, we get $\sigma_K \sim 2.4 \times 10^{-17}$ rad $\times$ cm^2, not far from the Faraday rotation cross section $\sigma_F = 2.4 \times 10^{-16}$ rad $\times$ cm^2, obtained by measuring the dc-Faraday rotation at the central energy of the probe spectrum. Thus, by amplification of Faraday rotation with a microcavity [29–31], a Faraday rotation angle of about $\frac{Q}{2\pi}\frac{\sigma_F}{d^2} \sim 10$ μrad can be obtained for a single Mn^{2+} ion, a cavity quality factor $Q \sim 3 \times 10^3$, and for a laser spot diameter $d = 1$ μm^2.

Finally, we report on measurements of T_2^{Mn} as a function of the effective Mn spin temperature T_{eff} [Fig. 4(c)]. T_{eff} is increased either by increasing the helium bath temperature T [32], or by increasing the excitation power P. At $T_{\text{eff}} >$ 10 K, we find $T_2^{\text{Mn}} \sim 15$ ns, as expected for dipolar broadening in a disordered spin system. Indeed, in the limiting case $\hbar\omega/k_B T \gg 1$ we find $(T_2^{\text{Mn}})^{-1} = \frac{8\pi^2}{9\sqrt{3}}\frac{(g\mu_B)^2}{\hbar} N_0 x S$, which gives $T_2^{\text{Mn}} \simeq 15$ ns for $x = 0.0011$ and $S = 5/2$. Setting $S = 1/2$ in this formula, one recovers within 4% the result of the theory of moments valid for disordered spins 1/2 [33]. This suggests that no strong temperature dependence is to be expected, while a marked decrease of T_2^{Mn} is observed below $T_{\text{eff}} = 10$ K. The clear correlation between the variations of T_2^{Mn} induced either by changing T, or by changing P, reflects the fact that T_2^{Mn} is mainly governed by the effective temperature of the Mn spin subsystem.

In conclusion, TRKR experiments reveal hyperfine beats of manganese spin in very diluted (Cd,Mn)Te. For magic orientations of the magnetic field, there is a direct correspondence between the measured Mn^{2+} spin precession frequency and the spin state of the Mn^{2+} nucleus. This provides a direct optical read-out of the Mn^{2+} nuclear spin, and opens a pathway for selective excitation of Mn^{2+} spins, conditioned by their nuclear spin state, by resonant spin amplification [34]. A model based on the spin Hamiltonian for local cubic symmetry accounts for the observed pattern of spin pulses. In addition, we find $T_2^{\text{Mn}} \sim$ 15 ns for temperatures between 10 to 30 K, as expected for the dipolar broadening mechanism. However, quite surprisingly T_2^{Mn} becomes shorter below 10 K. Finally, our experiments show that optical detection of a single Mn^{2+} spin is feasible by amplification of the Faraday rotation with a microcavity.

We thank F. Baboux for his participation to this work, M. Nawrocki for providing us with the sample, and C. Reibel for EPR experiments. D. S. enjoyed fruitful and stimulating discussions with M. Dyakonov. We wish to acknowledge the support of the french ANR research project SNS (Grant No. 2011-BS04-018 01), and of the Marie Curie research training network (MC-ITN) Clermont 4.

[1] R. Hanson, L. P. Kouwenhoven, J. R. Petta, S. Tarucha, and L. M. K. Vandersypen, Rev. Mod. Phys. **79**, 1217 (2007).
[2] M. S. Rudner, L. M. K. Vandersypen, V. Vuletić, and L. S. Levitov, Phys. Rev. Lett. **107**, 206806 (2011).
[3] J. M. Bao, A. V. Bragas, J. K. Furdyna, and R. Merlin, Phys. Rev. B **71**, 045314 (2005).
[4] N. Zhao, J. Honert, B. Schmid, M. Klas, J. Isoya, M. Markham, D. Twitchen, F. Jelezko, R.-B. Liu, H. Fedder *et al.*, Nat. Nanotechnol. **7**, 657 (2012).
[5] M. Kitagawa and M. Ueda, Phys. Rev. A **47**, 5138 (1993).
[6] A. Kuzmich, L. Mandel, and N. P. Bigelow, Phys. Rev. Lett. **85**, 1594 (2000).
[7] T. D. Ladd, D. Maryenko, Y. Yamamoto, E. Abe, and K. M. Itoh, Phys. Rev. B **71**, 014401 (2005).
[8] W. M. Witzel and S. Das Sarma, Phys. Rev. B **76**, 045218 (2007).
[9] D. R. McCamey, J. Van Tol, G. W. Morley, and C. Boehme, Science **330**, 1652 (2010).

[10] R. C. Myers, M. H. Mikkelsen, J. M. Tang, A. C. Gossard, M. E. Flatte, and D. D. Awschalom, Nat. Mater. **7**, 203 (2008).
[11] Y. Léger, L. Besombes, J. Fernández-Rossier, L. Maingault, and H. Mariette, Phys. Rev. Lett. **97**, 107401 (2006).
[12] E. Baudin, E. Benjamin, A. Lemaître, and O. Krebs, Phys. Rev. Lett. **107**, 197402 (2011).
[13] M. Goryca, T. Kazimierczuk, M. Nawrocki, A. Golnik, J. A. Gaj, P. Kossacki, P. Wojnar, and G. Karczewski, Phys. Rev. Lett. **103**, 087401 (2009).
[14] M. Blume and R. Orbach, Phys. Rev. **127**, 1587 (1962).
[15] J. Lambe and C. Kikuchi, Phys. Rev. **119**, 1256 (1960).
[16] S. A. Crooker, J. J. Baumberg, F. Flack, N. Samarth, and D. D. Awschalom, Phys. Rev. Lett. **77**, 2814 (1996).
[17] S. A. Crooker, D. D. Awschalom, J. J. Baumberg, F. Flack, and N. Samarth, Phys. Rev. B **56**, 7574 (1997).
[18] R. Akimoto, K. Ando, F. Sasaki, and T. Tani, J. Appl. Phys. **84**, 6318 (1998).
[19] C. Camilleri, F. Teppe, D. Scalbert, Y. G. Semenov, M. Nawrocki, M. Dyakonov, J. Cibert, S. Tatarenko, and T. Wojtowicz, Phys. Rev. B **64**, 085331 (2001).
[20] W. Low, *Paramagnetic Resonance in Solids, Solid State Physics* (Academic Press, New York and London, 1960).
[21] Not to be confused with the spinning magic angle in NMR experiments.
[22] The sample is oriented with a precision of $\pm 2°$.
[23] A. Nakamura, D. Paget, C. Hermann, C. Weisbuch, G. Lampel, and B. Cavenett, Solid State Commun. **30**, 411 (1979).
[24] M. Dyakonov, X. Marie, T. Amand, P. Le Jeune, D. Robart, M. Brousseau, and J. Barrau, Phys. Rev. B **56**, 10412 (1997).
[25] Y. G. Semenov, Phys. Rev. B **67**, 115319 (2003).
[26] D. D. Awschalom, M. R. Freeman, N. Samarth, H. Luo, and J. K. Furdyna, Phys. Rev. Lett. **66**, 1212 (1991).
[27] M. T. Causa, M. Tovar, S. B. Oseroff, R. Calvo, and W. Giriat, Phys. Lett. **77A**, 473 (1980).
[28] D. J. Hilton and C. L. Tang, Phys. Rev. Lett. **89**, 146601 (2002).
[29] S. Ghosh, W. H. Wang, F. M. Mendoza, R. C. Myers, X. Li, N. Samarth, A. C. Gossard, and D. D. Awschalom, Nat. Mater. **5**, 261 (2006).
[30] Y. Q. Li, D. W. Steuerman, J. Berezovsky, D. S. Seferos, G. C. Bazan, and D. D. Awschalom, Appl. Phys. Lett. **88**, 193126 (2006).
[31] J. Berezovsky, M. H. Mikkelsen, N. G. Stoltz, L. A. Coldren, and D. D. Awschalom, Science **320**, 349 (2008).
[32] At $T \geq 6$ K, T_{eff} could not be measured, hence we assume $T = T_{\text{eff}}$.
[33] C. Kittel and E. Abrahams, Phys. Rev. **90**, 238 (1953).
[34] J. M. Kikkawa and D. D. Awschalom, Phys. Rev. Lett. **80**, 4313 (1998).
[35] D. P. Halliday, M. D. G. Potter, J. T. Mullins, and A. W. Brinkman, J. Cryst. Growth **220**, 30 (2000).